Macroporous Monoliths of Functional Perovskite Materials through Assisted Metathesis

Eric S. Toberer,[†] James C. Weaver,[‡] K. Ramesha,[†] and Ram Seshadri*,[†]

Materials Department and Materials Research Laboratory, and Department of Molecular, Cellular and Developmental Biology and Materials Research Laboratory, University of California Santa Barbara, Santa Barbara, California 93106

Received November 6, 2003. Revised Manuscript Received March 9, 2004

Solid-state reactions between metal sulfates and metal oxides (assisted by K_2CO_3) have been used to prepare two classes of important perovskite materials: ferroelectric $PbTiO_3$ and the catalyst/magnetic/fuel-cell material $La_{1-x}Sr_xMnO_3$ ($x = 0.0$ and 0.3). K_2CO_3 helps to drive the reaction by forming highly stable K_2SO_4 and CO_2. Performing the reactions within solid monoliths and then dissolving out K_2SO_4 crystals in water permit macroporous materials to be obtained. The monoliths possess connected, open porosity with characteristic pore sizes of the order of 5−30 μm. Imprinted on this macroporous structure is a second, smaller scale of porosity arising from the sintering together of particles with sizes in the 100−300-nm range. The reaction pathways have been followed by thermodiffractometry, and the products characterized by Rietveld refinement of powder X-ray diffraction patterns, by scanning electron microscopy, and by dc magnetization measurements.

Introduction

Inspired by periodic bicontinuous macroporous patterns observed in the skeletal plates of certain echinoid biominerals,[1,2] we have for some time been interested in the problem of developing template-free routes to (macro)porous inorganic materials. Toward this goal, we have developed a general strategy based on the phase segregation of inorganic materials that parallels the formation of porous Vycor glass,[3] Raney Nickel, and certain Millipore filter membranes. We have so far considered the decomposition of single-source precursors[4] into two immiscible oxide phases, followed by the selective removal of one of the phases as a general strategy for the preparation of macroporous inorganic monoliths. Intimate two-phase mixtures of oxide phases can also be prepared via combustion synthesis,[5] and the removal of one of the oxide phases can result in a macroporous monolith of the other. These methods, while of interest, are limited in the kinds of material systems to which they can be applied.

To prepare macroporous monoliths of more complex, *functional* inorganic materials, we have proposed a scheme based on metathesis of the kind[6]

$$AB + CD \rightarrow AC + BD \qquad (1)$$

Here, AC could be the desired phase and BD could be a sacrificial phase that is removed by leaching. If such a scheme were to be carried out in a solid monolith, it is conceivable that the resulting material could be rendered macroporous. In earlier work, we established that $PbZrO_3$ composites with other inorganic materials, as well as $PbZrO_3$ particles, could be obtained by metathetic reactions in the solid state.[6] In this contribution, we demonstrate a variant of solid-state metathesis that we refer to as "assisted metathesis" and use it to prepare the very important perovskite oxides $PbTiO_3$ and $La_{1-x}Sr_xMnO_3$ ($x = 0.0$ and 0.3) at reduced temperatures. The reaction schemes presented here should be compared with what is more traditionally referred to as metathesis, for example, the very exothermic reaction between $MoCl_5$ and Na_2S.[7] In addition, by performing the reaction in solid monoliths, and by leaching out the second component in water, macroporous materials are obtained. Figure 1 displays a scheme of what has been achieved here.

In closely related work, Epple and Herzberg[8] have previously demonstrated the formation of porous polyglycollides by the internal metathesis of sodium salts of chloroacetic acid, followed by removal of NaCl. Suzuki et al. have prepared porous $CaZrO_3$/MgO composites by the reactive sintering of dolomite and ZrO_2[9] and porous $CaZrO_3/MgAl_2O_4$ composites by the reactive sintering of dolomite, ZrO_2, and Al_2O_3.[10]

* To whom correspondence should be addressed. E-mail: seshadri@mrl.ucsb.edu. Fax: (805) 893 8797.
[†] Materials Department and Materials Research Laboratory.
[‡] Department of Molecular, Cellular and Developmental Biology and Materials Research Laboratory.

(1) Meldrum, F. C.; Seshadri, R. *J. Chem. Soc., Chem. Commun.* **2000**, 29.
(2) Seshadri, R.; Meldrum, F. *Adv. Mater.* **2000**, *12*, 1149.
(3) Levitz, P.; Ehret, G.; Sinha, S. K.; Drake, J. M. *J. Chem. Phys.* **1991**, *95*, 6151.
(4) Rajamathi, M.; Thimmaiah, S.; Morgan, P.; Seshadri, R. *J. Mater. Chem.* **2001**, *11*, 2489.
(5) Panda, M.; Rajamathi, M.; Seshadri, R. *Chem. Mater.* **2002**, *14*, 4762.
(6) Panda, M.; Seshadri, R.; Gopalakrishnan, J. *Chem. Mater.* **2003**, *15*, 1554.
(7) Wiley, J.; Kaner, R. *Science* **1992**, *255*, 1093.
(8) Epple, M.; Herzberg, O. *J. Mater. Chem.* **1997**, *7*, 1037.
(9) Suzuki, Y.; Morgan, P. E. D.; Ohji, T. *J. Am. Ceram. Soc.* **2000**, *83*, 2091.
(10) Suzuki, Y.; Morgan, P. E. D.; Ohji, T. *Mater. Sci. Eng. A* **2001**, *304*, 780.

10.1021/cm0303540 CCC: $27.50
Published on Web 04/24/2004

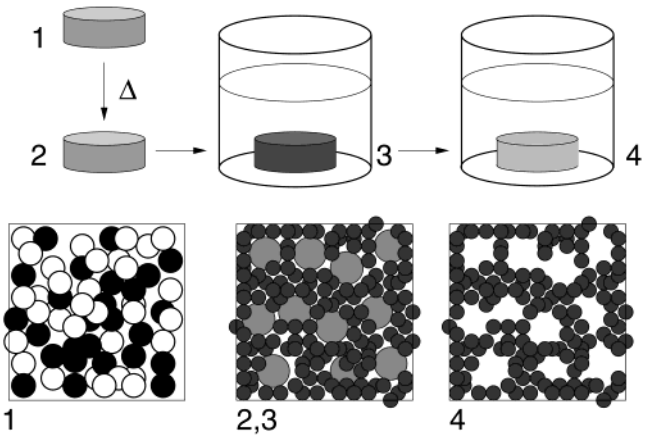

Figure 1. Scheme used to prepare macroporous monoliths from solid-state reactions. **1** is a pellet of a physical mixture of two or more reactants. **2** and **3** are pellets that comprise the two product phases. Removal by washing of one of the product phases results in a porous material **4**.

Perovskite lead titanate, $PbTiO_3$, is an important ferroelectric and piezoelectric material[11,12] continuing to find new applications, for example, as thin film acoustic sensors,[13] pyroelectric infrared detectors,[14] high-frequency resonators,[15] and optical planar waveguides.[16]

Recent efforts on preparing $PbTiO_3$ have been aimed at satisfying specific structural demands. Dense bulk $PbTiO_3$ has been formed through sol−gel[17] methods and fibers have been drawn from precursor gels of poly(acrylic acid).[18] Thin films have been fabricated via sol−gel,[19] electrostatic spray deposition,[20] plasma-enhanced CVD,[21] and magnetron sputtering.[22,23]

The hydrophone figure of merit of any material is a function of its piezo coefficients and of its compliance (mechanical properties) and is known to be enhanced when the material is rendered soft by making it porous.[24] This is the motive for preparing porous $PbTiO_3$. The preparation of other piezoelectric materials [such as the solid solution perovskites $(Pb,La)Zr_{1-x}Ti_xO_3$, PLZT] in porous form is an obvious next step. Macroporous $PbTiO_3$ has been prepared by infiltration of precursor material into an ordered 3D array of polystyrene beads followed by calcining,[25] in a process that is now well-established for the formation of ordered macroporous materials.[26]

An equally important class of perovskite oxide materials is derived from the rare-earth manganese oxides, exemplified by $LaMnO_3$. The unusual physical properties of substituted $LaMnO_3$ (in the series $La_{1-x}Sr_xMnO_3$, for example), including the strong coupling between magnetism and electrical transport, have been known for over 50 years since the pioneering work of Jonker and van Santen.[27] More recently, these compounds have been the focus of a great deal of attention following the finding that they display giant or colossal magnetoresistance.[28] Perovskite manganese oxides also find use in fuel cells as electrode materials[29] and in various catalytic processes such as the combustion of methane.[30]

In recent years, a number of groups have pursued the preparation of macroporous materials by backfilling templates such as organized colloidal spheres[31] and emulsions.[32] These routes result in highly ordered macroporous structures. The routes proposed in this work do not lead to highly ordered pores. However, they do permit the formation of complex functional materials as large as macroporous monoliths.

Experimental Section

The $PbTiO_3/K_2SO_4$ composite was prepared from powders (0.005 mole amounts) of K_2CO_3 (Fischer Scientific, 99.7%), TiO_2 (anatase, Aldrich, 99.9%), and $PbSO_4$ (Aldrich, 98%). The powders were ground by hand using an agate mortar and pestle to form an intimate mixture and pressed into a small pellet (10-mm diameter and approximately 3−4 mm in height). A force of about 5000 kg was applied in the process of making pellets. The pellet was calcined at 973 K in air for 12 h, following which it was ground, pressed, and fired again in air at 1048 K for 24 h.

The $La_{1-x}Sr_xMnO_3$ ($x = 0.0$ and 0.3)/K_2SO_4 composites were prepared from K_2CO_3, La_2O_3 (Aldrich, 99.99%), $SrCO_3$ (Spectrum Chemical, 99%), and $MnSO_4{\cdot}5H_2O$ (Aldrich, 98%) powders of the appropriate stoichiometry (0.005 mole basis). The powders were ground and pressed into a pellet, which was calcined at 1228 K for 12 h in air. The resulting pellet was then ground, pressed, and fired again for 24 h in air at 1228 K ($LaMnO_3$) or 1473 K ($La_{0.7}Sr_{0.3}MnO_3$).

For all three composites, the resulting sintered pellet was broken in half. One-half was placed in a beaker of deionized water at room temperature. The water was periodically replaced over the course of 3 days. The resulting monolith was dried in an air oven at 353 K for 12 h.

Powder X-ray diffraction (XRD) was recorded on a Scintag X2 diffractometer employing $\theta-2\theta$ geometry and Cu Kα radiation, operating at 45 kV and 35 mA, with a step size of 0.015° 2θ and step time of 8.5 s per step. Thermodiffraction (TDXRD) measurements were performed on a thin pressed pellet of the reactants, using a Bruker D8 Advance instrument (platinum heating stage, position-sensitive detector) with a 2° 2θ/min scan rate. The temperature was ramped in 25 K steps starting from 300 to 960 K (for $PbTiO_3$) or 1100 K (for the manganese oxides). Each scan was approximately 20 min and there was no pause between scans. Rietveld refinements of powder XRD data made use of the XND Rietveld code.[33] Thermogravimetry and thermal analysis measurements of the

(11) Lines, M. E.; Glass, A. M. *Principles and Applications of Ferroelectrics and Related Materials*; Clarendon Press: Oxford, 1977.
(12) Jona, F.; Shirane, G. *Ferroelectric Crystals*; Pergamon Press: New York, 1962.
(13) Chang, C.; Lin, W. *Ultrasonics* **2000**, *37*, 585.
(14) Yoshiike, N.; Morinaka, K.; Hashimoto, K.; Kawaguri, M.; Tanaka, S. *Sens. Actuators* **1999**, *77*, 199.
(15) Yoo, J.; Oh, D. *Sens. Actuators A* **2003**, *195*, 55.
(16) Urlacher, C.; Marty, O.; Plenet, J.; Serughetti, J.; Mugnier, J. *Thin Solid Films* **1999**, *349*, 61.
(17) Tartaj, J.; Moure, C.; Lascano, L.; Duran, P. *Mater. Res. Bull.* **2001**, *36*, 2301.
(18) Fan, C.; Ciardullo, D.; Huebner, W. *Mater. Sci. Eng. B* **2003**, *100*, 1.
(19) Bao, D.; Yao, X.; Wakiya, N.; Shinozaki, K.; Mizutani, N. *Mater. Sci. Eng.* **2002**, *B94*, 269.
(20) Huang, H.; Yao, X.; Wu, X.; Wang, M.; Zhang, L. *Microelectric Eng.* **2003**, *66*, 688.
(21) Tong, M.; Dai, G.; Gao, D. *Mater. Lett.* **2000**, *46*, 60.
(22) Zhao, Q.; Fan, Z.; Tang, Z.; Meng, X.; Song J.; Wang, G.; Chu, J. *Surf. Coat. Technol.* **2002**, *160*, 173.
(23) Stankus, V.; Dudonis, J.; Pranevicius, L.; Pranevicius, L.; Milcius, D.; Templier, C.; Riviere, J. *Thin Solid Films* **2003**, *426*, 78.
(24) Newnham, R. E. *MRS Bull.* **1993**, *18*, 27.
(25) Gundiah, G.; Rao, C. N. R. *Solid State Sci.* **2000**, *2*, 877.
(26) Holland, B.; Blanford, C.; Do, T.; Stein, A. *Chem. Mater.* **1999**, *11*, 795.
(27) Jonker, G. H.; van Santen, H. *Physics* **1950**, *16*, 599.
(28) Rao, C. N. R.; Cheetham, A. K.; Mahesh, R. *Chem. Mater.* **1996**, *8*, 2421.
(29) Nikravech, M.; Rousseau, F.; Morvan, D.; Amouroux, J. *J. Phys. Chem. Solids* **2003**, *64*, 1771.
(30) Cimino, S.; Pirone, R.; Lisi, L. *Appl. Catal., B* **2002**, *35*, 243
(31) Velev, O. D.; Kaler, E. W. *Adv. Mater.* **2000**, *12*, 531.
(32) Imhof, A.; Pine, D. J. *Nature* **1997**, *389*, 948.

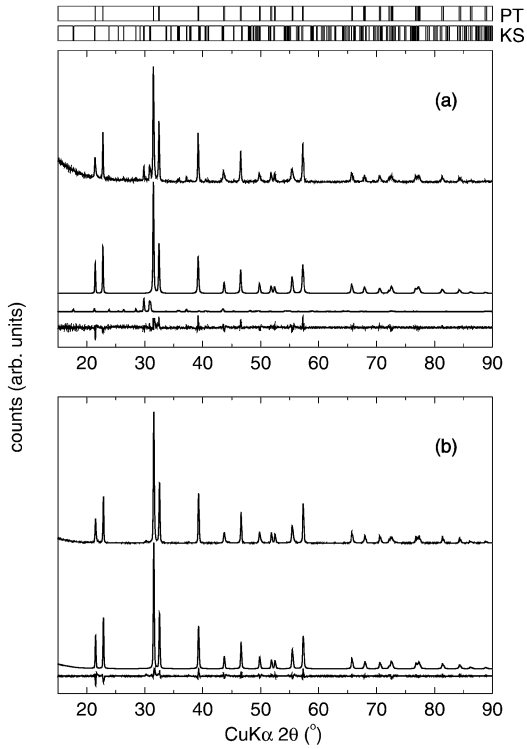

Figure 2. (a) Powder XRD pattern and two-phase Rietveld fits to the structures of tetragonal $PbTiO_3$ and β-K_2SO_4. The traces from top to bottom are data, fit to $PbTiO_3$ (background-corrected) fit to β-K_2SO_4, and difference profile. Vertical markers at the top indicate expected peaks positions for $PbTiO_3$ (PT) and β-K_2SO_4 (KS). (b) Data and Rietveld fit and difference profile of the washed $PbTiO_3$ sample.

unreacted powders and the resulting (washed) material were obtained on a Mettler TGA/STGA 851E. Scanning electron microscopy was performed using a JEOL6300F microscope equipped with an Oxford Inca X-ray system for energy-dispersive X-ray (EDX) analysis. The pellet was broken into smaller fragments, and the interior fracture surfaces of the pellet were imaged. Samples were mounted on double-sided carbon tape and gold-coated. The magnetic properties of a small pellet of the porous $La_{0.7}Sr_{0.3}MnO_3$ sample were studied using a Quantum Design MPMS 5XL SQUID magnetometer operated between 5 and 380 K.

Results and Discussion

$PbTiO_3$ Reaction and Product Formation. Heating well-ground mixtures of the reactants, K_2CO_3, TiO_2, and $PbSO_4$, at 973 K (12 h) and then at 1048 K (24 h) results in a composite of highly crystalline $PbTiO_3$ and K_2SO_4. Powder X-ray diffraction data for this composite are displayed in Figure 2a along with Rietveld fits to the tetragonal *P*4*mm* phase of $PbTiO_3$[34] and the orthorhombic β structure of K_2SO_4.[35] No other phase was found. Quantitative phase analysis using Rietveld scale factors[36] suggested a $PbTiO_3$:K_2SO_4 mole ratio of 53:47. Figure 2b displays the powder XRD pattern and Rietveld fit for the washed pellet obtained after leaching the $PbTiO_3$/K_2SO_4 composite with water. The only impurity observed in the pattern is a small amount of residual K_2SO_4 at a 2θ value of 30.1 °. A unit cell volume of 63.15(1) Å^3 was obtained from the Rietveld refinement, which is very close to the reported value of 63.3(3) Å^3.[34] This is an important verification of sample purity since substitution in the perovskite lattice (by potassium, for example) should result in a significant change (increase) in the cell volume. Sample purity was also confirmed by thermal analysis, which indicated a phase transition at 758 K, close to the reported temperature of 763 K for the tetragonal−cubic phase transition.[11]

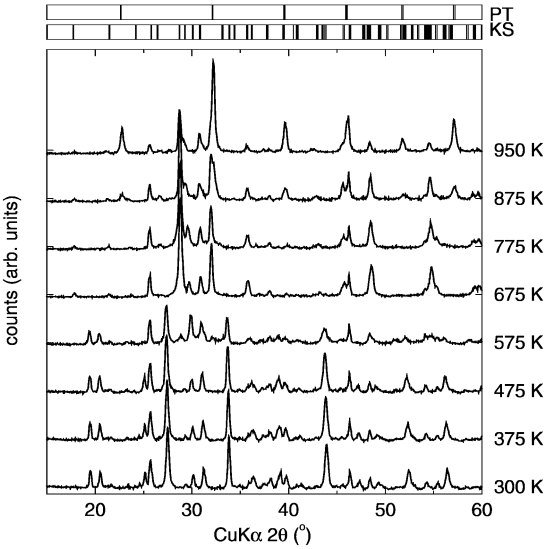

Figure 3. Thermodiffractometry of the assisted metathesis reaction forming $PbTiO_3$. The temperatures are indicated. Vertical lines at the top of the figure indicate the peak positions of cubic $PbTiO_3$ (PT) and β-K_2SO_4 (KS) refined for the 950 K pattern.

Figure 3 shows TDXRD patterns of reactants heated in air from room temperature to 950 K. Data were collected every 25 K, but for clarity, only 100 K intervals are displayed. Carbonate peaks, such as those around 20° 2θ burn off by 600 K. Peaks characteristic of $PbTiO_3$ emerge at around 875 K. The data at 950 K can be completely fit by the Rietveld method to a mixture of cubic $PbTiO_3$ and β-K_2SO_4.

When we attempted to assign the 300 K peaks in Figure 3 to the reactants, it became evident that, even at this low temperature, some reaction had taken place. A careful analysis of the room-temperature XRD pattern of a well-ground mixture of K_2CO_3 and $PbSO_4$ (Figure 4) showed reflections characteristic of β-K_2SO_4 (JC-PDF Card 24-0703), $PbCO_3$ (JC-PDF Card 05-0417), and $KPb_2(CO_3)_2(OH)_2$ (JC-PDF Card 37-0502). The reaction between K_2CO_3 and $PbSO_4$ therefore takes place at room temperature (with the intermediation of atmospheric moisture) according to

$$K_2CO_3 + PbSO_4 \rightarrow K_2SO_4 + PbCO_3 \qquad (2)$$

and

$$K_2CO_3 + 4PbCO_3 + H_2O \rightarrow 2KPb_2(CO_3)_2OH + CO_2 \qquad (3)$$

These results indicate the temperature of formation of $PbTiO_3$ is dictated by the reactivity of the TiO_2 since K_2SO_4 forms through a room-temperature metathesis.

(33) Bérar, J.-F.; Garnier, P. *NIST Spec. Pub.* **1992**, *846*, 212; freely available from the CCP14 website at http://www.ccp14.ac.uk.
(34) Megaw, H. D. *Crystal Structures: A Working Approach*; W.B. Saunders Co.: Philadelphia, 1973.
(35) Robinson, M. T. *J. Phys. Chem.* **1958**, *62*, 925.
(36) Brindley, G. W. *Philos. Mag.* **1945**, *36*, 347.

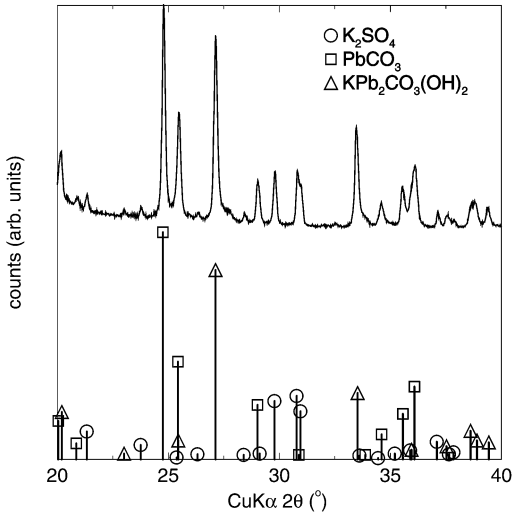

Figure 4. Powder XRD pattern of the products obtained at room temperature by grinding together the reactants K_2CO_3 and $PbSO_4$. The markers at the bottom of the plot indicate reflections from the appropriate JC-PDF files. These have been suitably scaled with relative heights maintained for each phase.

Table 1. Gibbs Free Energies of the Relevant Species Associated with $PbTiO_3$ Formation at 1000 K and the Room-Temperature Reaction of the Carbonates (All Data from Ref 37)

	ΔG_f (1000 K) (kJ mol^{-1})
$PbSO_4$	−548.953
TiO_2	−762.535
K_2CO_3	−861.496
$\Sigma_{Reactants}$	−2208.98
K_2SO_4	−1024.650
CO_2	−395.810
$PbTiO_3$	−914.036
$\Sigma_{Products}$	−2234.50
$\Delta_r G$ (1000 K)	−125.51
	ΔG_f (300 K) (kJ mol^{-1})
$PbSO_4$	−815.544
K_2CO_3	−1063.998
$\Sigma_{Reactants}$	−1879.54
$PbCO_3$	−624.927
K_2SO_4	−1318.951
$\Sigma_{Products}$	−1943.88
$\Delta_r G$ (300 K)	−64.336

Analysis of the thermodynamics of the $PbTiO_3/K_2SO_4$ reaction provides an explanation for the surprisingly low formation temperature of the $PbTiO_3$. The Gibbs free energy of formation at 1000 K of the reactants and products can be found in the standard work by Barin,[37] and the values are listed in Table 1. The reaction is indeed quite exothermic at 1000 K, with $\Delta_r G = -136.3$ kJ mol^{-1}; much of the contribution to the negative $\Delta_r G$ comes from the formation of K_2SO_4 and CO_2, justifying our use of the term "assisted metathesis". At 300 K, eq 2 also proceeds spontaneously, with $\Delta_r G = -64.3$ kJ mol^{-1}.[37]

$PbTiO_3$ Morphology. SEM images of the sintered $PbTiO_3/K_2SO_4$ pellet are displayed in Figure 5a,c. A cross section of the pellet reveals a surface composed of dense, well-sintered grains with crystallite sizes on the order of 300−500 nm. Scattered throughout this matrix are larger grains between 15 and 30 μm. The images displayed in Figure 5b,d show a cross section of the washed pellet. A spongelike network of $PbTiO_3$ remains, with pores in the 15−30-μm range. The matrix between these large pores remains quite dense, indicating that K_2SO_4 predominately aggregates into large grains and that the 300−500-nm grains are $PbTiO_3$. This is confirmed by EDX in the panels of Figure 6. Figure 6a displays an image where a few large grains are surrounded by a number of smaller grains. Figure 6b is an EDX mapping of K and S in this image, and Figure 6c is a mapping of Pb. From the maps, it is clear that the largers grains correspond to K_2SO_4 while the smaller ones are of $PbTiO_3$. The presence of K and S in the small grain areas can be attributed to large K_2SO_4 grains under the surface and incomplete aggregation of the K_2SO_4. One possible explanation for the large difference in grain size is that K_2SO_4 is formed immediately upon grinding as noted previously. On the other hand, $PbTiO_3$ grain growth commences only at elevated temperatures.

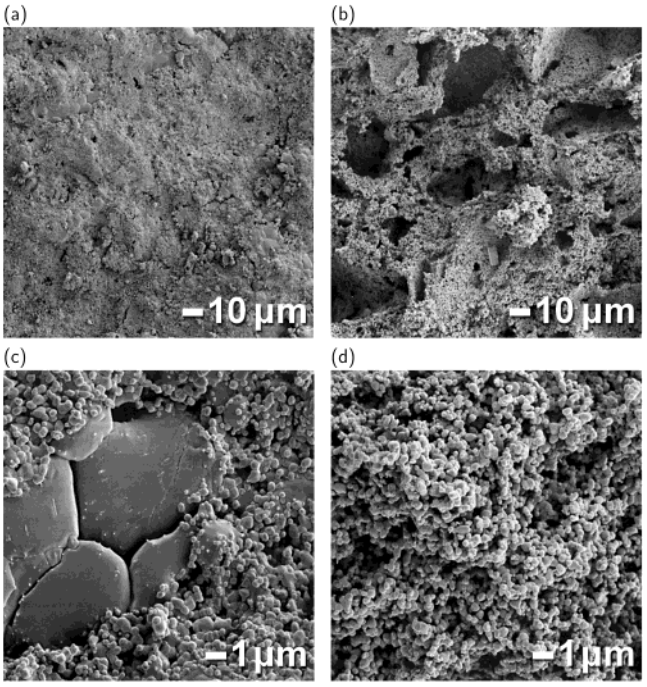

Figure 5. SEM images of the sintered composite pellet of $PbTiO_3$ and K_2SO_4 [(a) and (c)], and of the washed pellet, after removal of the K_2SO_4 [(b) and (d)].

For this route to be useful in the preparation of macroporous materials, it is important that the monoliths are robust. In the process of washing out the K_2SO_4, the pellets often crumble completely. This is alleviated by sintering the pellet for 24 h at 1048 K. The use of a flux such as LiF (between 0.5 and 5 wt %) are also found to be helpful in producing strong pellets.[9]

$La_{1-x}Sr_xMnO_3$ (x = 0.0 and 0.3) Reaction and Product Formation. Formation of $La_{1-x}Sr_xMnO_3/K_2SO_4$ occurred readily by heating the well-mixed reactants K_2CO_3, La_2O_3, $SrCO_3$, and $MnSO_4 \cdot 5H_2O$ at 1228 K (12 h) and then at 1228 K ($LaMnO_3$) or 1473 K ($La_{0.7}Sr_{0.3}MnO_3$). In performing Rietveld fits to the powder diffraction data (Figure 7a,b), it was found that the $R\bar{3}cH$ structure of cation-deficient $LaMnO_3$[38] resulted

(37) Barin, I. *Thermochemical Data of Pure Substances*, 3rd ed.; VCH Weinheim, 1995.

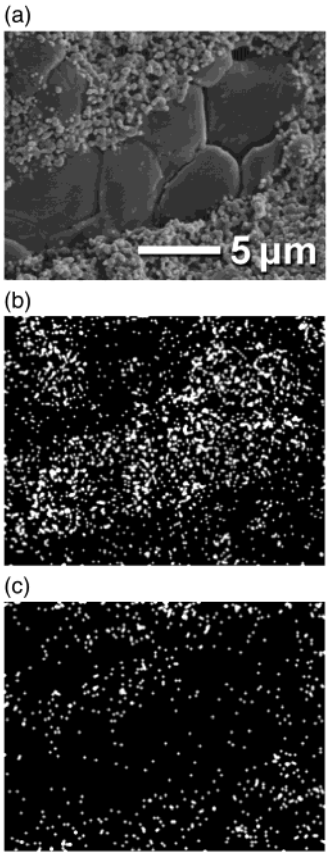

Figure 6. (a) SEM image of a portion of the sintered $PbTiO_3/K_2SO_4$ pellet showing some large crystallites flanked by smaller ones. (b) EDX mapping of regions with K and S. (c) EDX mapping of regions with Pb.

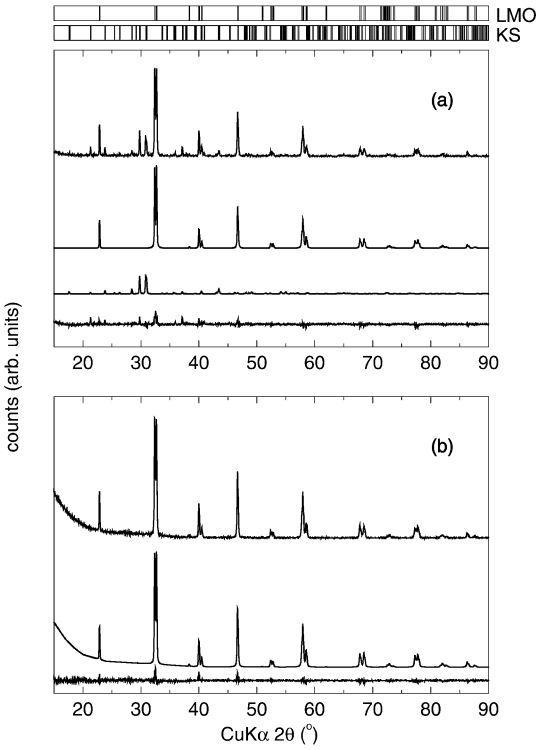

Figure 7. (a) Two-phase Rietveld fit of the powder XRD pattern of the sintered $LaMnO_3/K_2SO_4$ composite (LMO/KS). (b) Rietveld fit of the washed sample after removal of K_2SO_4.

in a better fit than did the orthorhomic structure of the stoichiometric compound.[39] Quantitative phase analysis

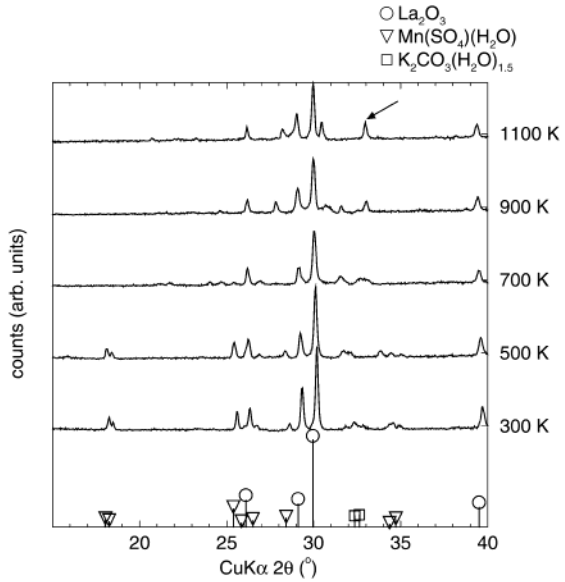

Figure 8. Thermodiffractometry of the assisted metathesis reaction forming $LaMnO_3$. The temperatures are indicated. The arrow indicates the main perovskite reflection. The markers at the bottom of the plot indicate reflections from the appropriate JC-PDF files. These have been suitably scaled with relative heights maintained for each phase as in Figure 4.

of the mixed phase sample (Figure 7a) using the Rietveld scale factors suggested a mole ratio of $LaMnO_3$ to K_2SO_4 of 54:46. The washed sample (Figure 7b) revealed no other phase than rhombohedral $LaMnO_3$. The unit cell volume of the $LaMnO_3$ was found to be 353.03(3) Å^3, close to the value of 352.1 Å^3 reported in a neutron diffraction study of $La_{0.96}Mn_{0.96}O_3$.[38]

Powder XRD data of the $La_{0.7}Sr_{0.3}MnO_3/K_2SO_4$ composite could be well-fitted by the structures of rhombohedral perovskite and β-K_2SO_4. The plots are provided in the Supporting Information. Quantitative phase analysis suggested a perovskite:K_2SO_4 ratio of 56:44. In the washed product, the only phase present is the rhombohedral perovskite, for which the La:Sr ratio could be refined to 0.72(1):0.28(1). This suggests the starting 0.7:0.3 La:Sr stoichiometry is maintained during the reaction. The unit cell volume of the $La_{0.7}Sr_{0.3}MnO_3$ was determined to be 351.40(2) Å^3 which corresponds well with previous reports.

TDXRD patterns were obtained for the $LaMnO_3$ and $La_{0.7}Sr_{0.3}MnO_3$ reactants heated in air from room temperature to 1100 K. Data were collected every 25 K, but for clarity, only 200 K intervals are displayed for the formation reaction for $LaMnO_3$ in Figure 8. Similar data for the formation of $La_{0.7}Sr_{0.3}MnO_3$ are included as Supporting Information. In both reactions, we find a peak at a 2θ value of 32.5° developing at 700 K (the peak is indicated in the figure with an arrow) corresponding to the main perovskite phase.

A striking difference between the two systems is the presence of the 30.2° 2θ La_2O_3 in the reaction, yielding $LaMnO_3$ (Figure 8). This peak remains through 1100 K. In the reaction to form, $La_{0.7}Sr_{0.3}MnO_3$, this peak

(38) Cheetham, A. K.; Rao, C. N. R.; Vogt, T. *J. Solid State Chem.* **1996**, *126*, 337.

(39) Rodríguez-Carvajal, J.; Hennion, M.; Moussa, F.; Moudden, A. H.; Pinsard, L.; Revcolevschi, A. *Phys. Rev. B* **1998**, *57*, R3189.

Table 2. Gibbs Free Energies of the Relevant Species Associated with $La_{1-x}Sr_xMnO_3$ ($x = 0$, 0.3) Formation (All Data from Ref 37 Unless Indicated)

	ΔG_f (1000 K) (kJ mol^{-1})
La_2O_3	−1507.667
$MnSO_4$	−704.398
K_2CO_3	−861.496
$SrCO_3$	−952.201
$\Sigma_{Reactants}$	
$x = 0.0$	−2319.73
$x = 0.3$	−2379.24
K_2SO_4	−1024.650
CO_2	−395.810
$La_{1-x}Sr_xMnO_3$ [*]	−1187.569
$\Sigma_{Products}$	
$x = 0.0$	−2608.04
$x = 0.3$	−2726.77
$\Delta_r G$ (1000 K)	
$x = 0.0$	−288.31
$x = 0.3$	−347.53

[a] ΔG_f calculated for $x = 0$ using data provided in ref 40 as explained in the text. We assume that Sr substitution ($x = 0.3$) leaves ΔG_f unchanged.

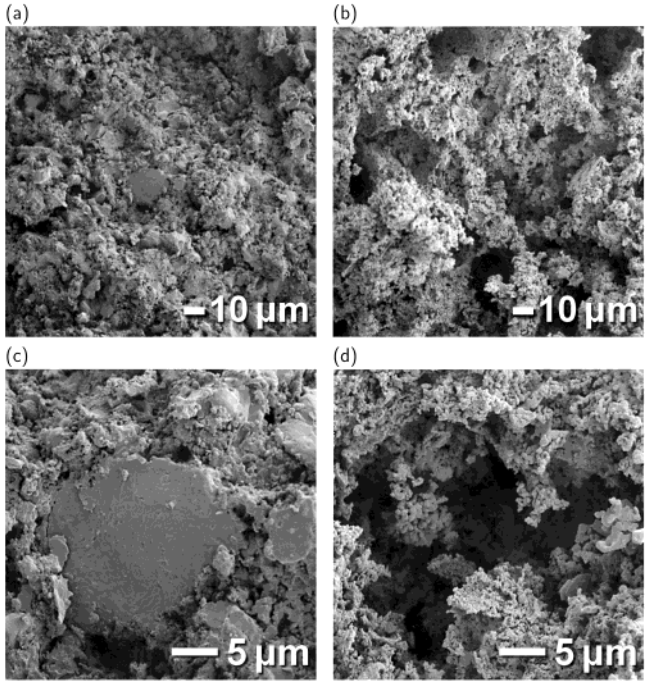

Figure 9. SEM images of [(a) and (c)] the sintered composite pellet of $LaMnO_3$ and K_2SO_4, and of the washed pellet, after removal of the K_2SO_4 [(b) and (d)].

disappears by 450 K and instead intermediate peaks can be matched with "La_2SrO_x" (JC-PDF Card 42-0343), the formation of which explains the distinct nature of reactivity.

The assisted metathesis schemes for the manganese perovskites are highly exothermic. Using thermochemical data from Barin[37] and data on $LaMnO_3$ from Navrotsky,[40] we obtain for the $LaMnO_3$ reaction a 1000 K $\Delta_r G$ of −288.31 kJ mol^{-1}. Assuming that $La_{0.7}Sr_{0.3}MnO_3$ has the same ΔG_f at 1000 K as $LaMnO_3$, its formation by the assisted metathesis route is associated with a $\Delta_r G$ of −347.53 kJ mol^{-1}. These data are summarized in Table 2.

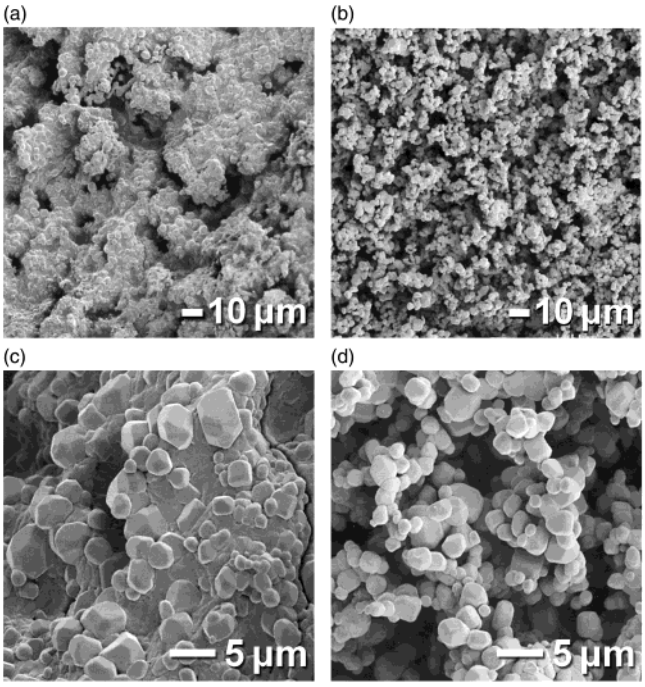

Figure 10. SEM images of [(a) and (c)] the sintered composite pellet of $La_{0.7}Sr_{0.3}MnO_3$ and K_2SO_4, and of the washed pellet, after removal of the K_2SO_4 [(b) and (d)].

$LaMnO_3$ Morphology. The microstructure of the sintered $LaMnO_3/K_2SO_4$ composite composites were imaged using SEM. The images, at different magnifications, are displayed in panels (a) and (c) of Figure 9. The composite $LaMnO_3/K_2SO_4$ in cross section revealed a dense collection of crystallites that are 300−500 nm in size, in which larger (10−20 μm) particles are embedded. As for the case of $PbTiO_3$ formation, the perovskite grains are the smaller ones, whereas the large crystals correspond to K_2SO_4. EDX mapping of K, S, La, and Mn (provided as Supporting Information) supports our assignment of these phases. The monolith that results from washing out K_2SO_4 in water reflects the difference in sizes of the two phases. Washed $LaMnO_3$ (Figure 9b,d) displays a sponge structure with distinct, physically separated, 10−20-μm pores.

$La_{0.7}Sr_{0.3}MnO_3$ Morphology and Magnetization. There are distinct differences in the microstructure of the $La_{0.7}Sr_{0.3}MnO_3/K_2SO_4$ pellet when compared with the $LaMnO_3/K_2SO_4$ pellet. In the $La_{0.7}Sr_{0.3}MnO_3/K_2SO_4$ system (which has been sintered at a higher temperature) we found 1−5-μm particles with quite sharp facets. In contrast, the $LaMnO_3$ particles were 300−500 nm. The difference in morphology could arise from the sintering temperature being above the melting point of K_2SO_4 (1342 K).[41] One possibility, therefore, is that K_2SO_4 melts and coats the $La_{0.7}Sr_{0.3}MnO_3$ crystallites. Indeed, when we attempted an EDX mapping of the metals and S on the $La_{0.7}Sr_{0.3}MnO_3/K_2SO_4$ pellet, we found these elements to be almost homogeneously dstributed, in a manner quite distinct from $PbTiO_3/K_2SO_4$ and $LaMnO_3/K_2SO_4$ systems.

In the $La_{0.7}Sr_{0.3}MnO_3$ system, removal of K_2SO_4 leads to a monolith having 5-μm pores with open connectivity (Figure 10b,d). In a comparison of $LaMnO_3$ and

(40) Laberty, C.; Navrotsky, A.; Rao, C. N. R.; Alphonse, P. *J. Solid State Chem.* **1999**, *145*, 77.

(41) Lide, D. R. *CRC Handbook of Chemistry and Physics*, 80th ed.; CRC Press: Boca Raton, FL, 2000.

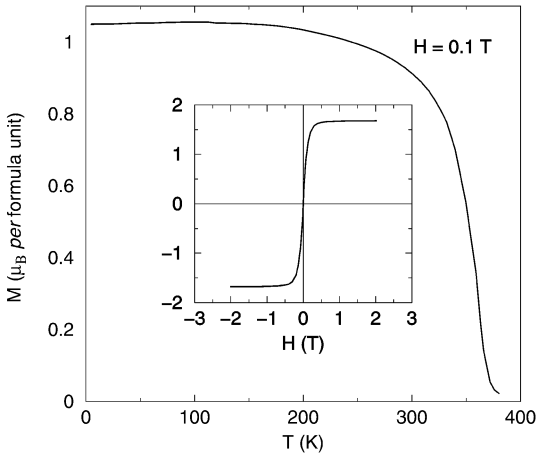

Figure 11. Temperature dependence of the field-cooled magnetization of the washed $La_{0.7}Sr_{0.3}MnO_3$ sample. The data were acquired in a 100 Oe field on warming after cooling under the same field from the room temperature. The inset is a magnetization loop acquired at 5 K.

$La_{1-x}Sr_xMnO_3$, the very different pore structures can be attributed to the different crystallite sizes of the sacrificial K_2SO_4 phase in the composites. The much larger K_2SO_4 crystallites seen in the composite with $LaMnO_3$ result in the washed material having large pores and thick walls. In the case of $La_{0.7}Sr_{0.3}MnO_3$, the walls are thinner and the pores smaller. So while $LaMnO_3$ has essentially isolated pores only connected via submicrometer pores between the grains, the pores in $La_{0.7}Sr_{0.3}MnO_3$ are separated by walls one to two grains thick, leading to a more open porosity.

Figure 11 displays the temperature dependence of the dc magnetization of a small (approximately 10 mg) monolith of the porous $La_{0.7}Sr_{0.3}MnO_3$. Data were acquired on warming under a 0.1 T field from 5 to 380 K, after cooling under a 0.1 T field. A sharp transition to ferromagnetism is seen at around 370 K. This corresponds to what is known of the magnetic phase diagram of $La_{1-x}Sr_xMnO_3$ for $x = 0.3$.[42] The inset in this figure displays a magnetization loop acquired at 5 K. There is almost no hysteresis in the sample. The saturation magnetization is reduced from the expected spin-only value of 3.7 μ_B per formula unit to about 1.7 μ_B, but the sharpness of the ferromagnetic transition as well as the shape of the hysteresis loop suggest no other magnetic phase is present.

Conclusion

We have demonstrated novel solid-state reactivity in the preparation of important functional perovskite materials, as well as a new and general route to preparing porous monoliths of inorganic materials. The method is based on assisted solid-state metathesis performed within monoliths, where one of the products is a sacrificial phase (chosen for its ease of solubility as well as the thermodynamic driving force it provides). As a next step, we hope to (i) extend the uses of such assisted metathesis to other functional (perhaps perovskite-related) materials, (ii) attempt greater control over pore size, and (iii) explore the uses of such porous materials.

Acknowledgment. E.S.T. is supported by the National Science Foundation IGERT program under the award DGE-9987618. This work was partially supported by the MRL program of the National Science Foundation under the Award No. DMR00-80034, and the authors made use of MRL facilities under Award No. DMR 93 32716. R.S. would like to acknowledge a Junior Faculty Grant from the UCSB Academic Senate. The authors acknowledge discussions with S. Stemmer, P. E. D. Morgan, and F. F. Lange. Katheryn Whitehead (NSF-RISE Undergraduate Intern) contributed to the project in its initial stages.

Supporting Information Available: Additional figures (PDF). This material is available free of charge via the Internet at http://pubs.acs.org.

CM0303540

(42) Imada, M.; Fujimori, A.; Tokura, Y. *Rev. Mod. Phys.* **1998**, *70*, 1039.